

LaSrCo_{0.5}Rh_{0.5}O_{3.25} and LaSrNi_{0.5}Rh_{0.5}O_{3.25}: Topochemically Reduced, Mixed Valence Rh(I)/Rh(III) Oxides.

Zheyang Xu[†], Robert G. Palgrave[‡], and Michael A. Hayward^{†*}

[†] Department of Chemistry, University of Oxford, Inorganic Chemistry Laboratory, South Parks Road, Oxford, OX1 3QR, UK.

[‡] Department of Chemistry, Department of Chemistry, University College London, 20 Gordon Street, London, WC1H 0AJ, UK.

ABSTRACT: Topochemical reduction of the $n = 1$ Ruddlesden-Popper phases LaSrCo_{0.5}Rh_{0.5}O₄ and LaSrNi_{0.5}Rh_{0.5}O₄ with Zr yields LaSrCo_{0.5}Rh_{0.5}O_{3.25} and LaSrNi_{0.5}Rh_{0.5}O_{3.25} respectively. Magnetization and XPS data reveal that while the rhodium centers in LaSrCo_{0.5}Rh_{0.5}O_{3.25} and LaSrNi_{0.5}Rh_{0.5}O_{3.25} have an average oxidation state of Rh²⁺ these are actually mixed valence Rh(I,III) compounds, with the disproportionation of Rh²⁺ driven by the favorability of locating d⁸ Rh^I and d⁶ Rh^{III} cations within square-planar and square-based pyramidal coordination sites respectively.

Introduction

As a class of compounds, complex metal oxides exhibit a wide range of useful chemical and physical properties which can, in general, be rationally tuned and optimized by modifying the chemical composition and/or crystal structure of the system. Of the parameters that combine to determine the chemical and physical behavior of complex oxides, the oxidation states of the metals present are among the most important.

A detailed study of the oxidation states adopted by metals in complex oxides reveals that a number of elements exhibit ‘disfavored’ oxidation states – those that appear to be thermodynamically accessible (sufficient lattice energy to overcome the required ionization energy) but which are rarely seen because they tend to disproportionate. For example, the binary oxides Pb₂O₃ and Bi₂O₄ have average metal oxidation states of Pb³⁺ and Bi⁴⁺ respectively. However, these compounds are better described as Pb^{II}Pb^{IV}O₃ and Bi^{III}Bi^VO₄, in which Pb³⁺ and Bi⁴⁺ have disproportionated to Pb^{II/IV} and Bi^{III/V} combinations.¹⁻²

The disproportionation of Pb³⁺ and Bi⁴⁺ can be attributed to the instability of the ns^1 electronic configuration with respect to an ns^0/ns^2 combination in heavy main group elements – a periodic trend often referred to as the ‘inert pair’ effect.³ However, similar disproportionations are observed for the oxidation states of transition metals, which do not appear to have ‘special’ electron counts. For example d⁴, Mn³⁺ cations are present in a large number of complex oxides, but the isoelectronic Fe⁴⁺ cation is often observed to disproportionate into mixtures of Fe^{III} and Fe^V centers at low-temperature in complex oxides,⁴⁻⁶ a behavior which is

attributed to strong hybridization between Fe 3d and O 2p bands in these extended solids.

Transition metal cations are also observed to disproportionate driven by the favorability of different coordination environment/d-electron count combinations. This behavior is especially prevalent for the 4d and 5d metals due to the enhanced ligand fields of the heavier elements. Thus, for example, while CuO adopts a structure in which paramagnetic d⁹, Cu²⁺ cations reside in apex-linked square-planar coordination,⁷ diamagnetic AgO is better described as Ag^IAg^{III}O₂,⁸ with the disproportionation of Ag²⁺ driven by the favorability of locating d¹⁰ Ag^I cations in linear coordination and d⁸ Ag^{III} cations in square-planar coordination sites.

Analogous coordination-site driven disproportionations are observed for 4d and 5d transition-metal cations with d⁷ electron counts, such as Pd³⁺ and Pt³⁺. In this case the favorability of square-planar coordinated d⁸ cations, combined with an octahedrally coordinated low-spin d⁶ cations, destabilize the d⁷ electron count, as seen in KPd₂O₃ (K₂Pd^{II}₃Pd^{IV}O₆),⁹ CdPt₃O₆ (CdPt^{II}Pt^{IV}₂O₆)¹⁰ and a number of other Pt and Pd oxides.¹¹⁻¹³

Here we report the topochemical reduction of a pair of rhodium-containing complex oxides, LaSrCo_{0.5}Rh_{0.5}O₄ and LaSrNi_{0.5}Rh_{0.5}O₄, to LaSrCo_{0.5}Rh_{0.5}O_{3.25} and LaSrNi_{0.5}Rh_{0.5}O_{3.25} respectively. These reduced phases have an average rhodium oxidation state of Rh²⁺, but are observed to be mixed valence Rh^I-Rh^{III} phases, analogous to the isoelectronic Pd^{II}-Pd^{IV} and Pt^{II}-Pt^{IV} oxides.

Experimental Section

Synthesis of $\text{LaSrM}_{0.5}\text{Rh}_{0.5}\text{O}_4$ ($M = \text{Co}, \text{Ni}$). Samples of $\text{LaSrCo}_{0.5}\text{Rh}_{0.5}\text{O}_4$ and $\text{LaSrNi}_{0.5}\text{Rh}_{0.5}\text{O}_4$ were prepared by a high-temperature ceramic method. Suitable stoichiometric ratios of La_2O_3 (99.999%, dried at 900 °C), SrCO_3 (99.994%), Rh_2O_3 (99.99%, dried at 850 °C) and Co_3O_4 (99.9985%) or NiO (99.998%) were ground together using an agate mortar and pestle, transferred into an alumina crucible, and then heated at a rate of 1 °C min⁻¹ to 1000 °C in air. Samples were then reground and pressed into pellets. Samples of $\text{LaSrCo}_{0.5}\text{Rh}_{0.5}\text{O}_4$ were then heated for 3 periods of 48 h at 1200 °C under flowing oxygen, with grinding between heating periods. Samples of $\text{LaSrNi}_{0.5}\text{Rh}_{0.5}\text{O}_4$ were heated for 3 periods of 48 h at 1300 °C under flowing oxygen, with grinding between heating periods.

Reduction of $\text{LaSrM}_{0.5}\text{Rh}_{0.5}\text{O}_4$ ($M = \text{Co}, \text{Ni}$) via Zr ‘getter’ reduction. Samples of $\text{LaSrCo}_{0.5}\text{Rh}_{0.5}\text{O}_4$ and $\text{LaSrNi}_{0.5}\text{Rh}_{0.5}\text{O}_4$ were reduced using a zirconium getter.¹⁴ Samples to be reduced were sealed in evacuated silica ampoules along with a glass ‘thimble’ containing 2 mole equivalents of powdered zirconium, such that the two powders shared an atmosphere but were not in physical contact. Small-scale test reactions were performed in which ~200 mg $\text{LaSrM}_{0.5}\text{Rh}_{0.5}\text{O}_4$ samples were heated at a rate of 2 °C min⁻¹ to temperatures in the range 450 °C – 520 °C and held there for 48 h to assess reactivity. This revealed that the optimum temperature for topochemical reduction was $T \sim 500$ °C, with no observable reaction occurring below $T = 480$ °C and non-topochemical decomposition reactions occurring above $T = 520$ °C. Samples of $\text{LaSrCo}_{0.5}\text{Rh}_{0.5}\text{O}_{4-x}$ and $\text{LaSrNi}_{0.5}\text{Rh}_{0.5}\text{O}_{4-x}$ characterized by neutron powder diffraction were prepared by heating ~2 g of $\text{LaSrCo}_{0.5}\text{Rh}_{0.5}\text{O}_4$ or $\text{LaSrNi}_{0.5}\text{Rh}_{0.5}\text{O}_4$ respectively with Zr for 3 periods of 5 days at 510 °C or 500 °C respectively, with samples being reground and the Zr replaced between heating periods.

Characterization. Sample purity and reaction progress were monitored by X-ray powder diffraction data which were collected using a PANalytical X’Pert diffractometer incorporating an X’celerator position sensitive detector (monochromatic $\text{Cu K}\alpha_1$ radiation). Data were collected from air sensitive samples under an inert atmosphere using homemade gas-tight sample holders. High-resolution synchrotron X-ray powder diffraction (SXR) data were collected using instrument I11 at the Diamond Light Source Ltd. SXR data were collected using Si-calibrated X-rays with an approximate wavelength 0.825 Å, from samples sealed in 0.3 mm diameter borosilicate glass capillaries. Neutron powder diffraction (NPD) data were collected using the POLARIS instrument (ISIS neutron source, U.K.) from samples sealed under argon and contained within vanadium cans. Rietveld profile refinement was performed using the GSAS suite of programs.¹⁵ DC magnetization data were collected using a Quantum Design MPMS SQUID magnetometer. Thermogravimetric measurements were performed by heating powder samples at a rate of 5 °C min⁻¹ under flowing dilute hydrogen, using a Mettler-Toledo MX1 thermogravimetric microbalance, and then cooling to 25 °C.

X-ray photoelectron spectroscopy (XPS) analysis was performed using a Kratos Axis SUPRA XPS fitted with a monochromated Al $\text{K}\alpha$ X-ray source (1486.7 eV), a spherical sector analyzer and 3 multichannel resistive plate, 128 channel delay line detectors. All data was recorded at 150 W and a spot size of 700 x 300 µm. Survey scans were recorded at a pass energy of 160 eV, and high-resolution scans recorded at a pass energy of 20 eV. Electronic charge neutralization was achieved using a magnetic immersion lens. Filament current = 0.27 A, charge balance = 3.3 V, filament bias = 3.8 V. All sample data was recorded at a pressure below 10⁻⁸ Torr and a room temperature of 294 K. Data was analyzed using CasaXPS v2.3.18PR1.0. C 1s sp³ peaks were calibrated to 284.8 eV. Air-sensitive samples were transferred into the spectrometer without exposure to air.

Results

Structural characterization of $\text{LaSrM}_{0.5}\text{Rh}_{0.5}\text{O}_4$ ($M = \text{Co}, \text{Ni}$). SXR data collected from $\text{LaSrCo}_{0.5}\text{Rh}_{0.5}\text{O}_4$ could be indexed on the basis of a body-centered tetragonal unit cell ($a = 3.879$ Å, $c = 12.518$ Å) consistent with the cation-disordered, $n = 1$ Ruddlesden-Popper structure reported previously.¹⁶ Refinement of a model based on this previously reported structure against the SXR data achieved a good fit, confirming sample purity and quality, as described in detail in the Supporting Information.

NPD data collected from $\text{LaSrNi}_{0.5}\text{Rh}_{0.5}\text{O}_4$ could also be indexed using a body-centered tetragonal unit cell ($a = 3.884$ Å, $c = 12.566$ Å). Refinement of a model based on the structure of $\text{LaSrCo}_{0.5}\text{Rh}_{0.5}\text{O}_4$, but with Co replaced by Ni, was refined against the NPD data achieving a good fit ($\chi^2 = 3.72$) as described in detail the Supporting Information. A detailed description of the physical properties of $\text{LaSrCo}_{0.5}\text{Rh}_{0.5}\text{O}_4$ and $\text{LaSrNi}_{0.5}\text{Rh}_{0.5}\text{O}_4$ will be given elsewhere.

Characterization of $\text{LaSrCo}_{0.5}\text{Rh}_{0.5}\text{O}_{4-x}$ and $\text{LaSrNi}_{0.5}\text{Rh}_{0.5}\text{O}_{4-x}$. SXR data collected from $\text{LaSrCo}_{0.5}\text{Rh}_{0.5}\text{O}_{4-x}$ and $\text{LaSrNi}_{0.5}\text{Rh}_{0.5}\text{O}_{4-x}$, prepared by Zr getter reduction from $\text{LaSrCo}_{0.5}\text{Rh}_{0.5}\text{O}_4$ and $\text{LaSrNi}_{0.5}\text{Rh}_{0.5}\text{O}_4$ respectively as described above, could be indexed using body-centered orthorhombic unit cells ($\text{LaSrCo}_{0.5}\text{Rh}_{0.5}\text{O}_{4-x}$: $a = 3.603$ Å, $b = 3.911$ Å, $c = 12.936$ Å; $\text{LaSrNi}_{0.5}\text{Rh}_{0.5}\text{O}_{4-x}$: $a = 3.580$ Å, $b = 3.927$ Å, $c = 12.810$ Å) consistent with topochemically reduced phases. Thermogravimetric data collected during the reductive decomposition of $\text{LaSrCo}_{0.5}\text{Rh}_{0.5}\text{O}_{4-x}$ and $\text{LaSrNi}_{0.5}\text{Rh}_{0.5}\text{O}_{4-x}$ to La_2O_3 , SrO , Rh and Co or Ni (confirmed by X-ray powder diffraction) under a 10:90 $\text{H}_2:\text{N}_2$ atmosphere, indicated mass losses of 3.37% and 3.30% respectively (Figures S3 and S4), consistent with sample stoichiometries of $\text{LaSrCo}_{0.5}\text{Rh}_{0.5}\text{O}_{3.26(1)}$ and $\text{LaSrNi}_{0.5}\text{Rh}_{0.5}\text{O}_{3.24(1)}$ respectively. Henceforth the two reduced phases will be referred to as $\text{LaSrCo}_{0.5}\text{Rh}_{0.5}\text{O}_{3.25}$ and $\text{LaSrNi}_{0.5}\text{Rh}_{0.5}\text{O}_{3.25}$.

In common with the SXR data, NPD data collected from $\text{LaSrCo}_{0.5}\text{Rh}_{0.5}\text{O}_{3.25}$ could be indexed using a body-centered orthorhombic unit cell, with extinction conditions consistent with the *Immm* space group (#71).

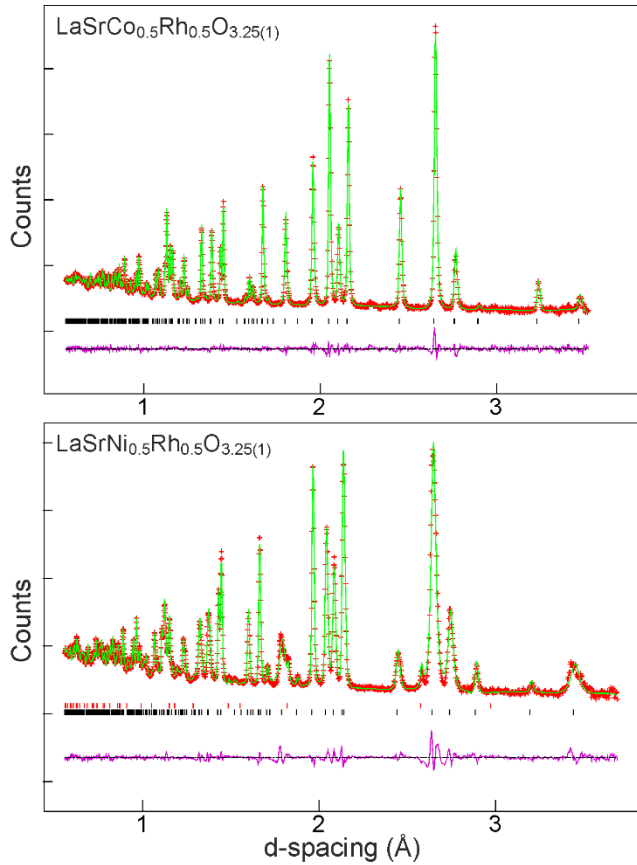


Figure 1. Observed calculated and difference plots from the structural refinement of $\text{LaSrCo}_{0.5}\text{Rh}_{0.5}\text{O}_{3.25}$ (top) and $\text{LaSrNi}_{0.5}\text{Rh}_{0.5}\text{O}_{3.25(1)}$ (bottom) against neutron powder diffraction data collected at room temperature using the detector bank centered at 92° . Black tick marks indicate peak positions for the majority phases, red tick marks for an SrO secondary phase.

Considering this, and the stoichiometry of the phase, a model based on the reported structure of $\text{Sr}_2\text{Fe}_{0.5}\text{Ru}_{0.5}\text{O}_{3.25}$ ¹⁷ was constructed (with the Fe/Ru solid solution replaced by Co/Rh) and refined against the NPD data. During the refinement all atomic positional and displacement parameters were refined freely along with the occupancy of the O(3) oxide ion residing at $(\frac{1}{2}, o, o)$. Close inspection of the displacement parameter of the O(2) anion site revealed that it was more than twice the size of displacement parameters of the O(1) and O(3) sites. This suggested that the O(2) site was disordered either side of the $x = o$ mirror plane, so the O(2) position was moved to a $(x, \frac{1}{2}, o)$ position with half occupancy. This led to an improvement in the fit to the data ($\chi = 1.98$) and physically sensible displacement parameters. In the final refinement cycles the occupancy of the O(3) anion site refined to a value of 0.251(5) without constraint, consistent with the composition $\text{LaSrCo}_{0.5}\text{Rh}_{0.5}\text{O}_{3.26(1)}$ obtained from TGA data. There was no evidence for partial occupancy on any of the other anion sites. Full details of the refined structure of $\text{LaSrCo}_{0.5}\text{Rh}_{0.5}\text{O}_{3.25}$ are given in Table 1, with selected bond lengths in Table 2. A plot of observed and calculated data is shown in Figure 1 and Figure S5 in the Supporting Information.

Atom	x	y	z	Fraction	$U_{\text{iso}} (\text{\AA}^2)$
La/Sr	o	o	0.3571(1)	0.5/0.5	0.0087(1)
Co/Rh	o	o	o	0.5/0.5	0.0108(2)
O (1)	o	o	0.1676(1)	1	0.0147(1)
O (2)	0.043(1)	$\frac{1}{2}$	o	0.5	0.0153(1)
O (3)	$\frac{1}{2}$	o	o	0.251(5)	0.0148(2)

$\text{LaSrCo}_{0.5}\text{Rh}_{0.5}\text{O}_{3.25}$ - space group *Immm* (#71)
Formula mass: 359.45 g mol⁻¹, Z = 2
 $a = 3.6033(1) \text{ \AA}$, $b = 3.9118(1) \text{ \AA}$, $c = 12.9363(3) \text{ \AA}$,
Volume = 182.34(1) \AA^3
Radiation source: Time-of-flight Neutron Powder Diffraction, $0.5 < d\text{-space}/\text{\AA} < 8$.
Temperature: 298 K, ambient pressure.
 $\chi^2 = 1.98$; $wRp = 2.27\%$; $Rp = 3.26\%$.

Table 1. Structural parameters from the refinement of $\text{LaSrCo}_{0.5}\text{Rh}_{0.5}\text{O}_{3.25}$ against NPD data collected at room temperature.

Cation	Anion	$M = \text{Co}$	$M = \text{Ni}$
La/Sr	O(1) $\times 1$	2.451(2)	2.439(2)
	O(1) $\times 4$	2.678(1)	2.678(1)
	O(2) $\times (2 \times \frac{1}{2})$	2.476(3)	2.444(3)
	O(2) $\times (2 \times \frac{1}{2})$	2.692(3)	2.664(3)
	O(3) $\times (2 \times \frac{1}{4})$	2.691(1)	2.676(1)
M/Rh	O(1) $\times 2$	2.168(1)	2.148(1)
	O(2) $\times (4 \times \frac{1}{2})$	1.962(1)	1.970(1)
	O(3) $\times (2 \times \frac{1}{4})$	1.802(1)	1.790(1)

Table 2. Selected bond lengths (\AA) from the refined structures of $\text{LaSrM}_{0.5}\text{Rh}_{0.5}\text{O}_{3.25}$ phases.

NPD data collected from $\text{LaSrNi}_{0.5}\text{Rh}_{0.5}\text{O}_{3.25}$ could also be indexed using a body-centered orthorhombic unit cell, with extinction conditions consistent with the *Immm* space group (#71). Therefore, a structural model analogous to that used for $\text{LaSrCo}_{0.5}\text{Rh}_{0.5}\text{O}_{3.25}$ was refined against these data, following the same refinement strategy employed for $\text{LaSrCo}_{0.5}\text{Rh}_{0.5}\text{O}_{3.25}$. Close inspection of the NPD data revealed a series of weak diffraction peaks consistent with a small amount of SrO (1.2 wt %) in the sample, so this was added as a second phase to the model. The refinement proceeded smoothly to achieve a good fit ($\chi = 4.56$). In the final refinement cycles the occupancy of the O(3) anion site refined to a value of 0.246(5) without constraint, consistent with the composition $\text{LaSrNi}_{0.5}\text{Rh}_{0.5}\text{O}_{3.24(1)}$ obtained from TGA data. Full details of the refined structure of $\text{LaSrNi}_{0.5}\text{Rh}_{0.5}\text{O}_{3.25}$ are given in Table 3, with selected bond lengths in Table 2. A plot of observed and calculated data is shown in Figure 1 and Figure S6 in the Supporting Information.

Atom	x	y	z	Fraction	U_{iso} (\AA^2)
La/Sr	o	o	0.3581(1)	0.5/0.5	0.0056(1)
Ni/Rh	o	o	o	0.5/0.5	0.0091(2)
O (1)	o	o	0.1677(1)	1	0.0121(1)
O (2)	0.044(1)	1/2	o	0.5	0.0110(1)
O (3)	1/2	o	o	0.246(5)	0.0126(2)
LaSrNi _{0.5} Rh _{0.5} O _{3.25} - space group <i>Immm</i> (#71)					
Formula mass: 359.33 g mol ⁻¹ , Z = 2					
$a = 3.5808(2)$ \AA , $b = 3.9277(2)$ \AA , $c = 12.8107(7)$ \AA , Volume = 180.18(2) \AA^3					
Phase fraction: 98.8(1) weight percent					
SrO - space group <i>Fm-3m</i>					
Formula mass: 103.62 g mol ⁻¹ , Z = 4					
$a = 5.1584(5)$ \AA					
Phase fraction: 1.2(1) weight percent					
Radiation source: Time-of-flight Neutron Powder Diffraction, $0.5 < d\text{-space}/\text{\AA} < 8$.					
Temperature: 298 K, ambient pressure.					
$\chi^2 = 4.56$; $wRp = 3.75\%$; $Rp = 4.80\%$.					

Table 3. Structural parameters from the refinement of LaSrNi_{0.5}Rh_{0.5}O_{3.25} against NPD data collected at room temperature.

XPS data collected from LaSrCo_{0.5}Rh_{0.5}O_{3.25} and LaSrNi_{0.5}Rh_{0.5}O_{3.25} are shown in Figure 2. It is clear that the Rh 3d_{5/2} and Rh 3d_{3/2} emission peaks for both reduced compounds are split, corresponding to the presence of two rhodium oxidation states. The Rh 3d spectra were fitted with one doublet representing each Rh oxidation state. For each doublet, 70% Gaussian 30% Lorentzian components were used and Rh 3d_{5/2} and 3d_{3/2} were constrained in area in a 3:2 ratio. The doublet separation was fixed at 4.71 eV. The two components of each doublet were initially constrained to have equal FWHM, and after a reasonable fitting was achieved, the 3d_{3/2} FWHM was allowed to increase slightly to account for the Coster-Kronig broadening expected in this core line.

For LaSrCo_{0.5}Rh_{0.5}O_{3.25} we find Rh 3d_{5/2} components with binding energies of 307.0 eV and 308.3 eV, for LaSrNi_{0.5}Rh_{0.5}O_{3.25} we find Rh 3d_{5/2} components at binding energies of 307.0 eV and 308.4 eV. In both cases, the lower binding energy component has a lower FWHM. This has been seen previously with Rh compounds.¹⁸ In each case, the higher energy component matches well with Rh₂O₃, and so we assign this peak as Rh^{III}.¹⁸ The peak close to 307 eV is in the region reported for Rh metal, although our model does not require asymmetric components that are present in elemental Rh. Rh^I molecular compounds have been reported with Rh 3d_{5/2} binding energy of 307.3 eV,¹⁹ but we are not aware of XPS studies of any rhodium oxides containing Rh^I. It is certainly possible that the Rh^I oxide peak will be at similar binding energy to the Rh metal peak, as is seen in other late transition metals such as Ag and Cu.

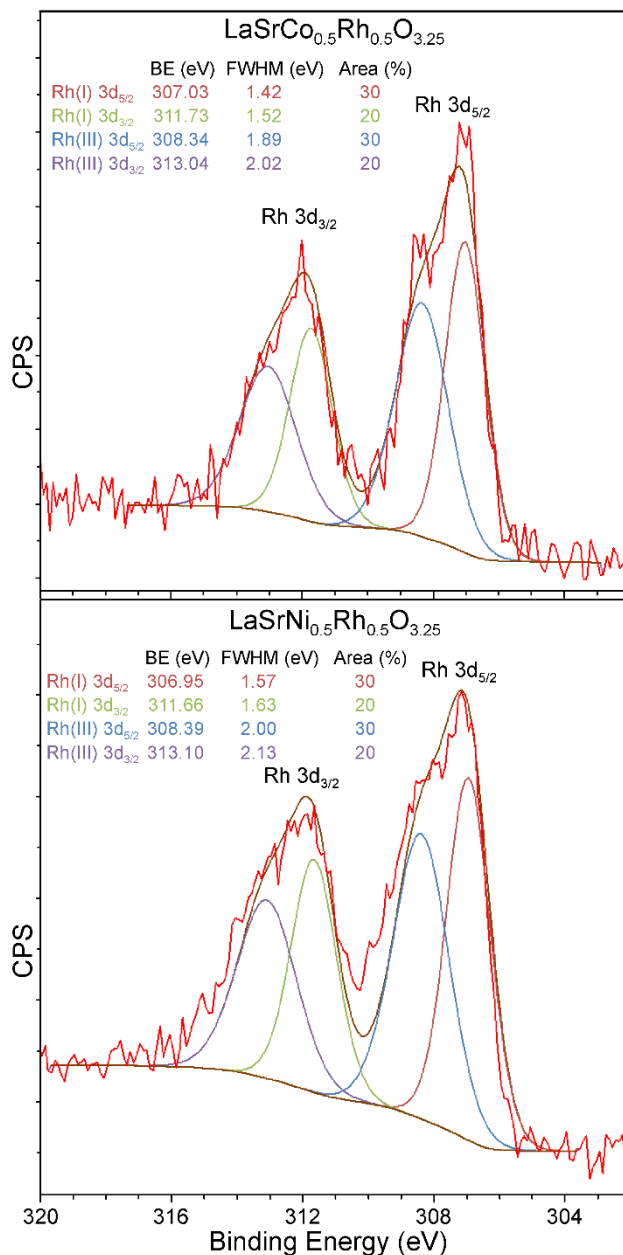


Figure 2. XPS collected from LaSrCo_{0.5}Rh_{0.5}O_{3.25} and LaSrNi_{0.5}Rh_{0.5}O_{3.25}. Peaks from the Rh 3d_{5/2} and Rh 3d_{3/2} emissions are fit by 2 components each, corresponding to Rh^I and Rh^{III}.

For both samples, the area of the Rh^I and Rh^{III} doublets were constrained to be equal. These constraints led to a good fit to the data, and similar values of binding energy and FWHM across the two samples, showing that the presence of an equal amount of Rh^I and Rh^{III} is consistent with the XPS measurements.

Magnetization data collected from LaSrCo_{0.5}Rh_{0.5}O_{3.25} and LaSrNi_{0.5}Rh_{0.5}O_{3.25} at room temperature indicate that samples contain small amounts (< 0.1 wt %) of ferromagnetic Co and Ni respectively. Therefore magnetization data were collected using a ‘ferromagnetic subtraction’ technique described in the Supporting Information, which utilizes the fact that the magnetization of Co and Ni saturate in applied fields greater than 2T.

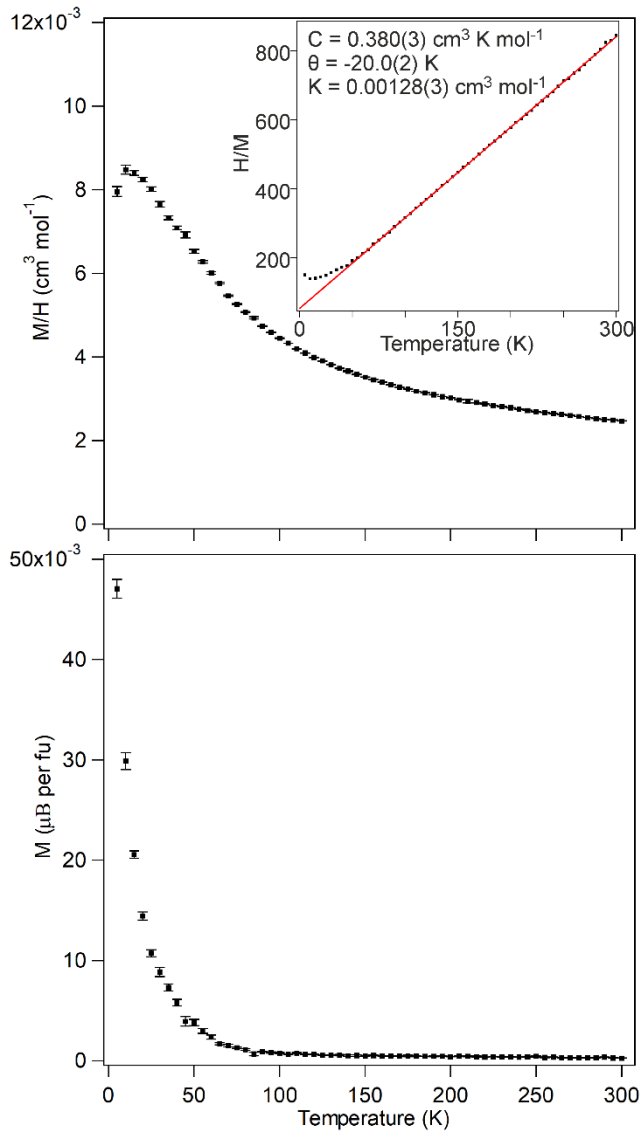


Figure 3. Paramagnetic susceptibility (top) and saturated ferromagnetic moment (bottom) of $\text{LaSrCo}_{0.5}\text{Rh}_{0.5}\text{O}_{3.25}$ plotted as a function of temperature. Inset shows fit to the Curie-Weiss law in the range $75 < T/\text{K} < 300$.

Figure 3 shows that the paramagnetic susceptibility of $\text{LaSrCo}_{0.5}\text{Rh}_{0.5}\text{O}_{3.25}$ follows the Curie-Weiss law ($\chi = C/(T - \theta) + K$) in the range $75 < T/\text{K} < 300$ to yield values of $C = 0.380(3) \text{ cm}^3 \text{K mol}^{-1}$, $\theta = -20.0(2) \text{ K}$ and $K = 1.28(3) \times 10^{-3} \text{ cm}^3 \text{mol}^{-1}$. Below 75 K the saturated ferromagnetic moment of $\text{LaSrCo}_{0.5}\text{Rh}_{0.5}\text{O}_{3.25}$ increases sharply and the susceptibility exhibits a maximum at $T = 10 \text{ K}$. These features of the data are consistent with a change to a magnetically ordered state below $T \sim 75 \text{ K}$.

Magnetization data collected from $\text{LaSrNi}_{0.5}\text{Rh}_{0.5}\text{O}_{3.25}$ shown in Figure 4 are qualitatively similar to the data from $\text{LaSrCo}_{0.5}\text{Rh}_{0.5}\text{O}_{3.25}$. Fitting the Curie-Weiss law in the range $25 < T/\text{K} < 300$ yields $C = 0.0761(8) \text{ cm}^3 \text{K mol}^{-1}$, $\theta = -8.01(5) \text{ K}$ and $K = 2.46(3) \times 10^{-4} \text{ cm}^3 \text{mol}^{-1}$. Below 25 K there is also a sharp increase in the saturated ferromagnetic moment of $\text{LaSrNi}_{0.5}\text{Rh}_{0.5}\text{O}_{3.25}$. Again, these features of the data are consistent with a change to a magnetically ordered state below $T \sim 25 \text{ K}$.

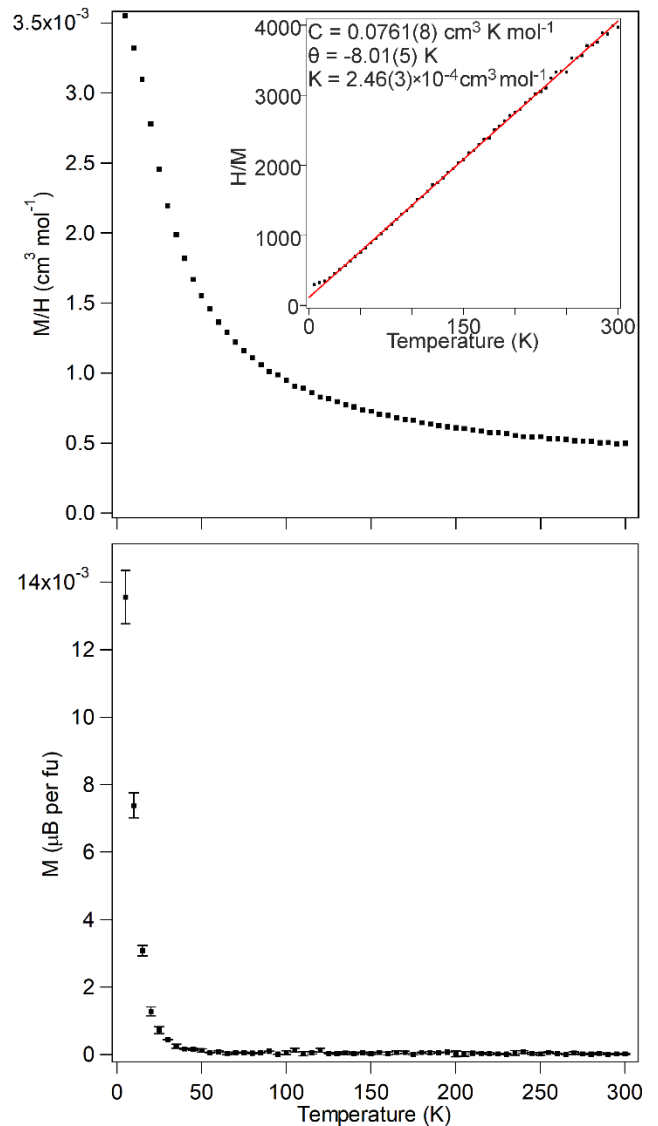


Figure 4. Paramagnetic susceptibility (top) and saturated ferromagnetic moment (bottom) of $\text{LaSrNi}_{0.5}\text{Rh}_{0.5}\text{O}_{3.25}$ plotted as a function of temperature. Inset shows fit to the Curie-Weiss law in the range $25 < T/\text{K} < 300$.

The addition of a weak ferromagnetic component to the magnetization of $\text{LaSrCo}_{0.5}\text{Rh}_{0.5}\text{O}_{3.25}$ and $\text{LaSrNi}_{0.5}\text{Rh}_{0.5}\text{O}_{3.25}$, at 75 K and 25 K respectively, suggests these materials adopt either a canted antiferromagnetic state or a spin-glass state at low temperature. NPD data collected from $\text{LaSrCo}_{0.5}\text{Rh}_{0.5}\text{O}_{3.25}$ and $\text{LaSrNi}_{0.5}\text{Rh}_{0.5}\text{O}_{3.25}$ at 5 K show no evidence for long range magnetic order, this excludes the possibility of a canted antiferromagnetic state. We therefore believe that it is likely that the changes in magnetic behavior observed at 75 K and 25 K for $\text{LaSrCo}_{0.5}\text{Rh}_{0.5}\text{O}_{3.25}$ and $\text{LaSrNi}_{0.5}\text{Rh}_{0.5}\text{O}_{3.25}$ respectively are transitions to spin-glass states. However, the presence of the ferromagnetic Co/Ni impurities prevents this being established definitively via magnetization measurements.

Discussion

Topochemical reduction of $\text{LaSrM}_{0.5}\text{Rh}_{0.5}\text{O}_4$ ($M = \text{Co}, \text{Ni}$) with a Zr oxygen getter yields $\text{LaSrM}_{0.5}\text{Rh}_{0.5}\text{O}_{3.25}$ phases as shown schematically in Figure 5a. The principal difference

between $\text{LaSrM}_{0.5}\text{Rh}_{0.5}\text{O}_4$ and $\text{LaSrM}_{0.5}\text{Rh}_{0.5}\text{O}_{3.25}$ is the partial occupancy of the O(3) anion site marked in pink in Figure 5a, which converts the (M/Rh)O₆ octahedra present in $\text{LaSrM}_{0.5}\text{Rh}_{0.5}\text{O}_4$ into a 1:1 disordered array of 5-coordinate, square-based pyramidal (M/Rh)O₅ and 4-coordinate, square-planar (M/Rh)O₄ coordination

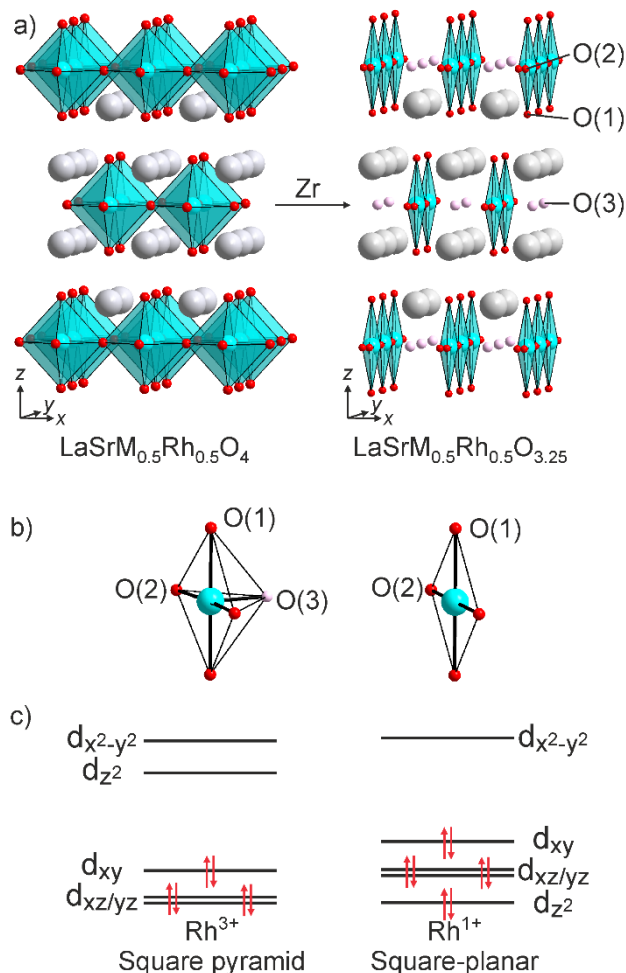


Figure 5. a) A schematic of the conversion of $\text{LaSrM}_{0.5}\text{Rh}_{0.5}\text{O}_4$ to $\text{LaSrM}_{0.5}\text{Rh}_{0.5}\text{O}_{3.25}$. Gray, blue, red and pink spheres represent La/Sr, M/Rh, O and partially occupied O positions respectively. b) square-based pyramidal and square-planar transition metal coordination sites in $\text{LaSrM}_{0.5}\text{Rh}_{0.5}\text{O}_{3.25}$. c) local electronic configurations of d⁶ Rh³⁺ and d⁸ Rh¹⁺ in square pyramidal and square-planar coordination respectively.

polyhedra in $\text{LaSrM}_{0.5}\text{Rh}_{0.5}\text{O}_{3.25}$, as shown in Figure 5b, which are equally occupied by M and Rh cations.

The $\text{LaSrM}_{0.5}\text{Rh}_{0.5}\text{O}_{3.25}$ stoichiometry of the reduced phases means that the average oxidation state of the M and Rh cations is +1.5, suggesting (Co/Ni)¹⁺, Rh²⁺ or (Co/Ni)²⁺, Rh¹⁺ combinations. However, spin-only calculations of the expected magnetic moments of these oxidation state combinations yield predicted moments which are much larger than the values determined from magnetization data, as described in detail in the Supporting Information. Resistivity measurements performed on cold-pressed powder samples indicate that both $\text{LaSrCo}_{0.5}\text{Rh}_{0.5}\text{O}_{3.25}$ and

$\text{LaSrNi}_{0.5}\text{Rh}_{0.5}\text{O}_{3.25}$ are highly insulating, eliminating itinerant electronic behavior as an explanation for the low moments.

The very small magnetic moment observed for both reduced phases suggests there is only a modest contribution from the Rh centers. When combined with the clear splitting of the Rh 3d XPS peaks for both reduced compounds this suggests a scenario in which the Co/Ni cations are in a monovalent oxidation state and the accompanying Rh²⁺ cations have disproportionated into a 1:1 ratio of Rh³⁺ and Rh¹⁺ which are located within the square-based pyramidal and square-planar coordination sites respectively, with S = 0 electronic configurations as shown in Figure 5c. The primary drive for this disproportionation is attributed to the crystal-field stabilization energy gained by the square-planar coordinated Rh cations adopting d⁸, S = 0 electronic configuration (Rh¹⁺) and the Rh cations in square-based pyramidal coordination sites adopting a low-spin d⁶ (Rh³⁺) configuration, which is advantageous compared to locating d⁷ Rh²⁺ in these two sites.

These low-spin, diamagnetic electronic configurations for rhodium yield predicted Curie constants of 0.1875 cm³ K mol⁻¹ for M = Ni, and either 0.25 or 0.5 cm³ K mol⁻¹ for M = Co (depending on the spin-state adopted by square-planar coordinated Co¹⁺) in broad agreement with the values of 0.0761(8) and 0.380(3) cm³ K mol⁻¹ observed for $\text{LaSrNi}_{0.5}\text{Rh}_{0.5}\text{O}_{3.25}$ and $\text{LaSrCo}_{0.5}\text{Rh}_{0.5}\text{O}_{3.25}$ respectively.

Further support for the disproportionation of Rh²⁺ comes from the XPS data. Figure 2 shows that the Rh 3d emission for both $\text{LaSrCo}_{0.5}\text{Rh}_{0.5}\text{O}_{3.25}$ and $\text{LaSrNi}_{0.5}\text{Rh}_{0.5}\text{O}_{3.25}$ are clearly split into two components which are assigned to Rh³⁺ and Rh¹⁺ as described above.

Analogous disproportionations to ‘avoid’ oxidation states with d⁷ electron counts are observed for other 4d and 5d transition metals. For example, KPd_2O_3 has an average Pd oxidation state of Pd^{2.5+}, suggesting a mixture of Pd²⁺ and Pd³⁺.⁹ However, close inspection of the crystal structure of this compound reveals it is better formulated as $\text{K}_2\text{Pd}^{\text{II}}_3\text{Pd}^{\text{IV}}\text{O}_6$, with d⁸ Pd²⁺ cations located in square-planar $\text{Pd}^{\text{II}}\text{O}_4$ units, and d⁶ Pd⁴⁺ cations located in octahedral $\text{Pd}^{\text{IV}}\text{O}_6$ units. Likewise, BiPd_2O_4 and $\text{Ba}_2\text{Hg}_3\text{Pd}_7\text{O}_{14}$ are better formulated as $\text{Bi}_2\text{Pd}^{\text{II}}_3\text{Pd}^{\text{IV}}\text{O}_8$ and $\text{Ba}_2\text{Hg}_3\text{Pd}^{\text{II}}_5\text{Pd}^{\text{IV}}_2\text{O}_{14}$ based on their crystal structures, which also contain distinct $\text{Pd}^{\text{II}}\text{O}_4$ and $\text{Pd}^{\text{IV}}\text{O}_6$ units.^{11, 13}

Similar behavior is also observed for the 5d member of group 11, platinum, with octahedral $\text{Pt}^{\text{IV}}\text{O}_6$ and square-planar $\text{Pt}^{\text{II}}\text{O}_4$ units observed in a wide range of $\text{M}^{2+}\text{Pt}^{\text{II}}\text{Pt}^{\text{IV}}_2\text{O}_6$ (M = Cd, Mn, Co, Zn, Ni, Mg) oxides.^{10, 12} However, to date analogous charge-separated Ir^I/Ir^{III} oxides have not been prepared. Reported topochemically reduced iridium oxides, such as $\text{Sr}_2\text{FeIrO}_4$, or $\text{Sr}_2\text{Co}_{0.5}\text{Ir}_{0.5}\text{O}_3$ are observed to contain d⁷ Ir²⁺ cations in square-planar coordination sites.²⁰⁻²¹ It is hard to say anything comprehensive about the different behavior of reduced Rh and Ir compounds given that, to the best of our knowledge, $\text{LaSrCo}_{0.5}\text{Rh}_{0.5}\text{O}_{3.25}$ and $\text{LaSrNi}_{0.5}\text{Rh}_{0.5}\text{O}_{3.25}$ are the first reports of extended oxides containing Rh in an oxidation state below Rh³⁺, and the small number of topochemically reduced iridium oxides reported. However, it is worth noting that if

LaSrCo_{0.5}Rh_{0.5}O₄ is treated under the same conditions required to convert Sr₂Fe^{III}Ir^VO₆ to Sr₂Fe^{II}Ir^{II}O₄ (CaH₂, 400 °C)²¹ it is converted to the Rh^{III} oxyhydride LaSrCo_{0.5}Rh_{0.5}O₃H,¹⁶ suggesting that the reduction of Rh³⁺ is more challenging than the corresponding reduction of Ir.

Conclusion

Topochemical reduction of the $n = 1$ Ruddlesden-Popper phases LaSrCo_{0.5}Rh_{0.5}O₄ and LaSrNi_{0.5}Rh_{0.5}O₄ with Zr yields LaSrCo_{0.5}Rh_{0.5}O_{3.25} and LaSrNi_{0.5}Rh_{0.5}O_{3.25} respectively. Analysis reveals that while the rhodium centers in the LaSrM_{0.5}Rh_{0.5}O_{3.25} phases have an average oxidation state of Rh²⁺ these are actually mixed valence Rh(I,III) compounds and are thus the first observation of Rh¹⁺ in an extended oxide.

The ‘disproportionation’ of Rh²⁺ in the LaSrM_{0.5}Rh_{0.5}O_{3.25} phases raises a number of questions about the factors controlling the extent of anion-deintercalation processes. Is the formation of the LaSrM_{0.5}Rh_{0.5}O_{3.25} a fortunate coincidence? That is to say, is it a fortunate coming together of the oxygen stoichiometry, crystal structure and transition-metal oxidation states to form a compound which provides a large kinetic barrier to further reduction to the corresponding LaSrM^I_{0.5}Rh^I_{0.5}O₃ phases? Or is the disproportionation indicative of a deeper instability of Rh²⁺? Further investigations will be required to clarify this point, but the results presented here hint at a rich oxide chemistry for low-valent, late transition metal oxides.

ASSOCIATED CONTENT

Supporting Information. Structural characterization of LaSrCo_{0.5}Rh_{0.5}O₄ and LaSrNi_{0.5}Rh_{0.5}O₄; Reductive thermogravimetric analysis of LaSrCo_{0.5}Rh_{0.5}O_{3.25} and LaSrNi_{0.5}Rh_{0.5}O_{3.25}; Additional data plots from the structural characterization of LaSrCo_{0.5}Rh_{0.5}O_{3.25} and LaSrNi_{0.5}Rh_{0.5}O_{3.25}; Description of the ‘ferrosbtraction’ procedure; discussion of the spin-state/oxidation-state combinations of LaSrM_{0.5}Rh_{0.5}O_{3.25} phases. This material is available free of charge via the Internet at <http://pubs.acs.org>.

AUTHOR INFORMATION

Corresponding Author

* michael.hayward@chem.ox.ac.uk

Author Contributions

The manuscript was written through contributions of all authors.

ACKNOWLEDGMENT

Experiments at the Diamond Light Source were performed as part of the Block Allocation Group award “Oxford Solid State Chemistry BAG to probe composition-structure-property relationships in solids” (EE13284). Experiments at the ISIS pulsed neutron facility were supported by a beam time allocation from the Science and Technology Facilities Council. The

XPS data collection was performed at the EPSRC National Facility for XPS (“HarwellXPS”), operated by Cardiff University and UCL, under Contract No. PR16195.

REFERENCES

- Bouvaist, J.; Weigel, D., Sesquioxide de plomb, Pb₂O₃. I. Determination de la structure. *Acta Cryst.* **1970**, A 26, 501 - 510.
- Kumada, N.; Kinomura, N.; Woodward, P. M.; Sleight, A. W., Crystal Structure of Bi₂O₄ with beta-Sb₂O₄-type Structure. *J. Solid State Chem.* **1995**, 116 (2), 281-285.
- Orgel, L. E., The Stereochemistry of B-subgroup Metals. 2. The Inert Pair. *Journal of the Chemical Society* **1959**, (DEC), 3815-3819.
- Romero, F. D.; Shimakawa, Y., Charge transitions in perovskite oxides containing unusually high-valent Fe. *Chem. Commun.* **2019**, 55 (26), 3690-3696.
- Takano, M.; Nakanishi, N.; Takeda, Y.; Naka, S.; Takada, T., Charge Disproportionation in CaFeO₃ studied with Mossbauer Effect. *Mater. Res. Bull.* **1977**, 12 (9), 923-928.
- Woodward, P. M.; Cox, D. E.; Moshopoulou, E.; Sleight, A. W.; Morimoto, S., Structural studies of charge disproportionation and magnetic order in CaFeO₃. *Phys. Rev. B* **2000**, 62 (2), 844-855.
- Åsbrink, S.; Norrby, L.-J., A Refinement of the Crystal Structure of Copper(II) Oxide with a Discussion of Some Exceptional E.s.d's. *Acta Cryst.* **1970**, B 26, 8 - 15.
- McMillan, J. A., Magnetic properties and crystalline structure of AgO. *J. Inorg. Nucl. Chem.* **1960**, 13, 28 - 31.
- Panin, R. V.; Khasanova, N. R.; Bougerol, C.; Schnelle, W.; Van Tendeloo, G.; Antipov, E. V., Ordering of Pd²⁺ and Pd⁴⁺ in the Mixed-Valent Palladate KPd₂O₃. *Inorg. Chem.* **2010**, 49 (4), 1295-1297.
- Prewitt, C. T.; Schwartz, K. B.; Shannon, R. D., Synthesis and Structure of Orthorhombic Cadmium Platinum Oxide, CdPt₃O₆. *Acta Crystallographica Section C-Crystal Structure Communications* **1983**, 39 (MAY), 519-521.
- Hansen, T.; Mullerbuschbaum, H., On the First Alkaline-Earth Mercurate(II)-Palladate(II,IV) - Ba₂Hg₃Pd₅2²⁺Pd₂4⁴⁺O₁₄. *Z. Anorg. Chem.* **1992**, 616 (10), 67-70.
- Schwartz, K. B.; Parise, J. B.; Prewitt, C. T.; Shannon, R. D., Structure and Crystal-Chemistry of Mixed-Valence Platinum Oxides - MnPt₃O₆, CoPt₃O₆, ZnPt₃O₆, MgPt₃O₆, NiPt₃O₆. *Acta Crystallogr. Sect. B-Struct. Commun.* **1983**, 39 (APR), 217-226.
- Yi, W.; Matsushita, Y.; Tanaka, M.; Belik, A. A., High-Pressure Synthesis, Crystal Structure, and Properties of BiPd₂O₄ with Pd²⁺ and Pd⁴⁺ Ordering and PbPd₂O₄. *Inorg. Chem.* **2012**, 51 (14), 7650-7656.
- Hayward, M. A., Soft chemistry synthesis of oxides. In *Comprehensive Inorganic Chemistry II*, Reedijk, J.; Poeppelemer, K. R., Eds. Elsevier: Oxford, 2013; Vol. 2, pp 417-453.
- Larson, A. C.; Von Dreele, R. B. *General Structure Analysis System*, Los Alamos National Laboratory Report LAUR 86-748: 2000.
- Jin, L.; Hayward, M. A., Rhodium-containing oxide-hydrides: covalently stabilized mixed-anion solids. *Chem. Commun.* **2019**, 55 (33), 4861-4864.
- Denis Romero, F.; Gianolio, D.; Cibin, G.; Bingham, P. A.; d'Hollander, J.-C.; Forder, S. D.; Hayward, M. A., Topochemical reduction of the Ruddlesden-Popper phases Sr₂Fe_{0.5}Ru_{0.5}O₄ and Sr₃(Fe_{0.5}Ru_{0.5})₂O₇. *Inorg. Chem.* **2013**, 52, 10920-10928.
- Abe, Y.; Kato, K.; Kawamura, M.; Sasaki, K., Rhodium and Rhodium Oxide Thin Films Characterized by XPS. *Surface Science Spectra* **2002**, 8, 117-125.
- Carvalho, M.; Wieserman, L. F.; Hercules, D. M., Spectroscopic Characterisation of Wilkinson Catalyst Using X-

Ray Photo-Electron Spectroscopy (ESCA). *Applied Spectroscopy* **1982**, 36 (3), 290-296.

20. Page, J. E.; Hayward, M. A., Structure and Magnetism of $(\text{La/Sr})_2\text{M}_{0.5}\text{Ir}^{\text{V}_{0.5}}\text{O}_4$ and Topochemically Reduced $(\text{La/Sr})_2\text{M}_{0.5}\text{Ir}^{\text{II}_{0.5}}\text{O}_3$ (M = Fe, Co) Complex Oxides. *Inorg. Chem.* **2019**, 58 (9), 6336-6343.

21. Page, J. E.; Morgan, H. W. T.; Zeng, D.; Manuel, P.; McGrady, J. E.; Hayward, M. A., $\text{Sr}_2\text{FeIrO}_4$: square-planar Ir(II) in an extended oxide. *Inorg. Chem.* **2018**, 57, 13577-13585.

SYNOPSIS TOC

Topochemical reduction of $\text{LaSrCo}_{0.5}\text{Rh}_{0.5}\text{O}_4$ and $\text{LaSrNi}_{0.5}\text{Rh}_{0.5}\text{O}_4$ with Zr yields $\text{LaSrCo}_{0.5}\text{Rh}_{0.5}\text{O}_{3.25}$ and $\text{LaSrNi}_{0.5}\text{Rh}_{0.5}\text{O}_{3.25}$ respectively. Magnetization and XPS data reveal that while the rhodium centers in $\text{LaSrCo}_{0.5}\text{Rh}_{0.5}\text{O}_{3.25}$ and $\text{LaSrNi}_{0.5}\text{Rh}_{0.5}\text{O}_{3.25}$ have an average oxidation state of Rh^{2+} these are actually mixed valence $\text{Rh}(\text{I,III})$ compounds, with the disproportionation of Rh^{2+} driven by the favorability of locating $d^8 \text{Rh}^{1+}$ and $d^6 \text{Rh}^{3+}$ cations within square-planar and square-based pyramidal coordination sites respectively.

For Table of Contents only:

